Atom Efficient PtCu Bimetallic Catalysts and Ultra Dilute Alloys for the Selective Hydrogenation of Furfural

Martin J. Taylor,[a] Simon K. Beaumont,[b] Mohammed J. Islam,[c] Sotirios Tsatsos,[d] Christopher A. M. Parlett,[e, f, g] Mark A. Issacs[h, i] and Georgios Kyriakou[d]*

[a] Energy and Environment Institute, University of Hull, Cottingham Road, Hull, HU6 7RX, United Kingdom

[b] Department of Chemistry, Durham University, Durham, DH1 3LE, United Kingdom

[c] Energy & Bioproducts Research Institute, Aston University, Aston Triangle, Birmingham, B4 7ET, United Kingdom

[d] Department of Chemical Engineering, University of Patras, Caratheodory 1, Patras GR 265 04, Greece

[e] Department of Chemical Engineering and Analytical Science, University of Manchester, Manchester, M1 3AL, United Kingdom

[f] University of Manchester at Harwell, Diamond Light Source, Harwell Campus, Didcot, OX11 0DE, United Kingdom

[g] Spectroscopy village, Diamond Light Source, Harwell Science and Innovation Campus, Didcot, OX11 0DE, United Kingdom

[h] Department of Chemistry, University College London, 20 Gordon Street, Kings Cross, London, WC1H 0AJ, United Kingdom

[i] Harwell XPS, Research Complex at Harwell, Rutherford Appleton Labs, Didcot, OX11 0FA, United Kingdom

Abstract

A range of Pt:Cu bimetallic nanoparticles were investigated for the liquid-phase selective hydrogenation of furfural, an important platform biomass feedstock. Alloying of the two metals had a profound effect on the overall catalytic activity, providing superior rates of reaction and achieving the needed high selectivity towards furfuryl alcohol. Furthermore, we investigated the catalytic activity of an Ultra Dilute Alloy (UDA) formed via the galvanic replacement of Cu atoms by Pt atoms on dispersed host Cu nanoparticles (atomic ratio Pt:Cu 1:20). This UDA, after overcoming an induction period, exhibits exceptionally high initial rates of hydrogenation under modest hydrogen pressures of 10 and 20 bar, rivalling the catalytic turnover for the monometallic Pt (containing 12 times more Pt), and outdoing the pure Cu or other compositions of bimetallic nanoparticle alloy catalysts. These atom efficient catalysts are ideal candidates for the valorization of furfural due to their activity and vastly greater economic viability.

KEYWORDS: Pt, Cu, Selective Hydrogenation, Furfural, Bimetallic Alloy, Ultra Dilute Alloy

Introduction

The push towards sustainable chemistry grows day-by-day. One such strategy is through the transformation of bio-renewable feedstocks, especially with regards to the production of value-added chemicals derived from lignocellulosic biomass wastes. Pyrolysis of the hemicellulose component from such biomass generates various oxygenates—one such molecule is furfural.[1, 2] More specifically, furfural is the product of direct dehydration of C_5 sugars[3-6] and is used effectively as an extractant to remove aromatic components from lubricants and diesel fuel.[7] It also has a role in the polymer industry as it can readily undergo acetalization and participate in various condensation reactions.[7, 8] Moreover, it is also used as an agricultural fungicide.[6, 7] Currently, the majority of furfural produced worldwide (~60 %) is hydrogenated to furfuryl alcohol (Scheme 1),[4, 6] a key intermediate for the manufacture of many fine chemicals and essential industrial compounds, such as adhesives, lubricants, and corrosion resistant coatings.[4-6, 9-11] The present industrial scale hydrogenation is a relatively small scale and hazardous process, using a copper chromite catalyst. Although providing a moderate activity and relatively high selectivity toward furfuryl alcohol, it requires harsh reaction conditions to be effective (~200 ^{o}C and ~30 bar).[4, 12] Over time the catalyst degrades and Cr(VI) is formed, causing both a hazard to workers and environmental danger, since the disposal of this substance is problematic and landfill is prohibited.[13, 14] An array of alternative metal catalysts have been used in the literature for the hydrogenation of furfural to furfuryl alcohol in both the liquid and vapour phase, examples being: Cu, Ni, Pd, Pt, Co, Rh, Ir and Ru.[10, 15-22] Pt has been shown previously to be highly active and selective at low reaction temperatures under a headspace hydrogen atmosphere in the liquid phase.[16] Additionally, Pt is also effective for the hydrogenation of furfural in the vapour phase and also under Ultra-High Vacuum (UHV) conditions on Pt(111).[23, 24] More recently, we have studied the formation of copper-based catalysts ranging from nanoparticles to small clusters and isolated Cu species supported on nanophased alumina in the catalytic liquid-phase hydrogenation of furfural. These catalysts were synthesized via a wet impregnation method using various copper precursors at two different loadings.[8] A high Cu loading led to the formation of well-defined nanoparticles, while a lower loading formed a highly dispersed phase consisting mostly of atomic and dimeric

Cu species on Al_2O_3. The catalytic reaction was found to be structure sensitive, promoting decarbonylation reactions with a low Cu loading.[8]

Previously, bimetallic catalysts (two different metals, which can either be miscible or immiscible, represented as a bulk alloy)[25] have been exploited for the hydrogenation of furfural. Some of these binary alloy systems consist of PtSn, PtGe, RhSn, NiSn, CuCo, PdCu, PdAg and PdRh.[11, 21, 26-29] However, the majority of alloy research does not consider the reduction of precious metal content, purely an alloy effect promoted by relatively high loadings of both metals, creating a difference in reaction selectivity.[27, 28, 30-32] It has been shown over recent years, that by depositing isolated catalytic entities on the surface of a metal nanoparticle, the properties of the parent particle can be enhanced dramatically via hydrogen spillover.[33] Isolated atomic entities on a host nanoparticle may provide reaction rate improvements as well as changes to product selectivities.

The aim of this work is to investigate the effects of precious metal dilution, in this case Pt, with a metal that is both cheap and not catalytically effective by itself at modest loadings. Cu as a catalyst for the reaction has only been found to be highly effective in the form of copper chromite, which (as outlined above) there is an urgent need to replace. However, in this form Cu has shown excellent selectivity towards furfuryl alcohol but also deactivation over time especially when used in the Cu/Cr_2O_3 form on an industrial scale.[34] Precious metals have been investigated in the literature, but not found practical application.[23, 35] The motivation for this study is to combine the Cu and Pt synergistically, providing high activities and selectivities toward useful products such as furfuryl alcohol from the furfural hydrogenation reaction, but without the expense of a high loaded precious metal catalyst. Previously PdCu nanoparticles have been shown to increase furfural conversion and selectivity towards furfuryl alcohol compared to monometallic Pd which is known for being unselective.[15] Across a number of studies, the reaction parameters used accommodate both high temperatures (80-160 ºC) and high metal loadings, with only minor Pd dilutions taking place (5 wt% □ 3 wt%). It was found that by alloying Cu with Pd, a significant decrease in tetrahydrofuran production took place.[30, 36, 37] PtNi is another alloy system that has been explored recently that has shown that Ni shifts the

selectivity towards C=C hydrogenation, favouring tetrahydrofurfuryl alcohol.[38] This is due to an alteration in the furfural adsorption profile, Wu and co-workers show that furfural adsorbs to the surface via a planer motif on Ni sites.[38]

In the present paper the catalytic hydrogenation of furfural is studied using bimetallic PtCu nanoparticles supported on γ-Al_2O_3 at varying Pt:Cu molar ratios to demonstrate the effect of precious metal dilution and the promotional effect induced by Pt on a relatively inactive metal component, Cu. Our previous work found that there was a mild particle-support interaction when depositing Pt on γ-Al_2O_3 which lead to a tight particle size distribution.[15] It has been shown previously that Pt nanoparticles of ~4 nm are optimal for the production of furfuryl alcohol.[39] Additionally, γ-Al_2O_3 is known to be mildly acidic, Lewis acidity gas been found to be beneficial for hydrogenation reactions.[40] This work will probe the synergistic effects of Pt and Cu in an alloyed state, scrutinizing a potentially more active/selective catalytic species Pt_xCu_{1-x}, through hydrogen spillover caused by the hydrogen activating metal, Pt.[41, 42] Additionally, to investigate the effect of Cu on the selectivity of the hydrogenation reaction. Finally, low dilution of Pt in Cu (as much as 1:20 atomic fraction, where galvanostatic replacement targets obtaining surface Pt atoms) is investigated, limiting wasted precious metal in the form of buried platinum atoms.

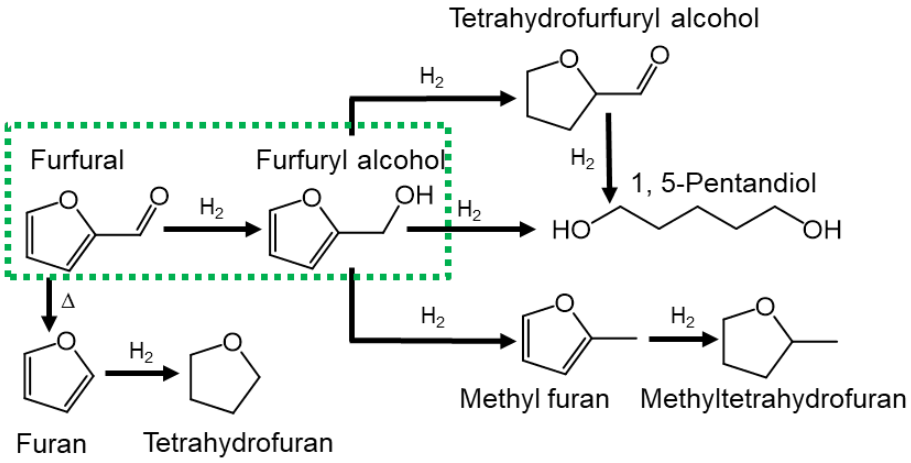

Scheme 1. General reaction scheme for the transformation of furfural, targeted reaction pathway is highlighted in a green square.

Experimental

Catalyst synthesis

Monometallic and Bimetallic nanoparticles: Colloidal Pt, Cu and PtCu nanoparticles were synthesized using a similar method to that we have employed previously.[16] To ensure bimetallic particles, subtle modifications were made to allow for a slow addition of the metal precursor solution. Varying molar ratios of $H_2PtCl_6.3H_2O$ (Alfa Aesar, 99.9%) and $Cu(NO_3)_2$ (Acros, 99%) were added to a 9:2 ratio of ethylene glycol and water in the presence of polyvinylpyrrolidone (PVP) (40000 MW, Alfa Aesar) and briefly sonicated until fully dissolved. This was followed by dropwise addition into a warm ethylene glycol solution (140 °C) containing NaOH (1 mL, 1 M) via syringe pump (World Precision Instruments, AL-4000 Programmable Syringe Pump) at 5 mL h^{-1}. Slowly, the colour of the solution turned from light brown to black for Pt and PtCu solutions, whereas the Cu solution changed from a light blue to brown. After full addition of the metal solution, the reaction mixture was stirred for an additional 20 min and then cooled to room temperature. Nanoparticles were isolated by the addition of acetone (three times the reaction volume) followed by subsequent centrifugation at 4000 rpm for 10 min, three times. The nanoparticles were then suspended in ethanol and supported on γ-Al_2O_3 (Alfa Aesar 99.5%, 32–40 m^2 g^{-1}). The support was not pretreated prior to nanoparticle deposition. Catalysts were dried under vacuo and then dried in an oven at 60 °C overnight. The monometallic and bimetallic powders of nominal Pt:Cu molar ratios 50:50 and 25:75 were transferred to a muffle furnace and heated at 3 °C min^{-1} in static air to 300 °C for 4 h to remove excess synthetic agents. Table 1 shows that although these intended nominal molar ratios were not achieved, the as synthesized 38:62 and 18:82 molar ratio catalysts cover a reasonably broad compositional range for catalyst testing.

Ultra Dilute Alloy: An atom efficient catalyst was synthesized by adopting a galvanic replacement method previously reported by Lucci et al.[43] Initially, a monometallic 1% Cu/γ-Al_2O_3 catalyst was generated by the same process described above, but following

calcination in air, the powder was reduced under H_2 flow at 300 °C for 3 h. The resulting material, ~1 g, was immediately added to 50 mL of HCl (2 mM) while under nitrogen protection. Galvanic replacement, the process where surface host atoms are replaced with a different metal, in this case Pt, was completed under constant stirring and refluxing at 100 °C where a low concentration of $H_2PtCl_6.3H_2O$ (Alfa Aesar, 99.9%) in H_2O was added to the mixture. After 20 min, the resulting material was separated via centrifuged (4000 rpm, 10 min), washed multiple times with deionized water (~300 mL) and dried in an oven at 60 °C overnight.

Characterization of catalysts

All samples were analysed using a Cs aberration-corrected JEOL 2100-F microscope at 200 kV, a HAADF detector and Gatan Ultrascan 4000 bright field camera operated by Digital Micrograph software. Further image analysis was carried out using ImageJ 1.52a software. Samples were dispersed in methanol and deposited on 300-mesh carbon-supported nickel grids and dried under ambient conditions. Metal contents were determined by Inductively Coupled Plasma Optical Emission Spectroscopy using a Thermo Scientific iCAP 7400 Duo, after microwave digestion of the samples in 5 mL HNO_3 (Fisher, 70%) and 100 mg NH_4F (Sigma Aldrich, ≥98.0%) at 190 °C (CEM–MARS microwave reactor) followed by dilution in 10% aqueous HNO_3. BET surface areas were determined via N_2 physisorption using a Quantachrome Nova 1200. Samples were degassed at 120 °C for 1 h prior to analysis by nitrogen adsorption at -196 °C. X-ray photoelectron spectra were acquired on a Kratos AXIS HSi spectrometer equipped with a charge neutralizer and dual anode, where an Al Kα excitation source (1486.7 eV), with energies referenced to adventitious carbon at 284.6 eV, samples were mounted onto carbon tape. Spectral fitting was performed using CasaXPS version 2.3.15 using a Shirley background where surface atomic compositions were calculated via correction for the appropriate instrument response factors. Powder X-ray diffraction experiments were performed on a Bruker D8 Advance diffractometer Cu K$\alpha_{1,2}$ radiation (40 mA and 40 kV, 0.02 mm Ni Kβ filter and 2.5° Soller slits). Diffractograms were collected in the Bragg-Brentano geometry with a step scan of 0.02° (1 s per step) and the samples were top-loaded into PMMA specimen holders. Subsequent peak assignment was based on the ICDD's PDF-2 2012 & ICSD databases. PXRD

derived particle sizes were estimated using the Scherrer equation based on the FWHM of the (111) metallic reflection using a Gaussian fit and shape factor of 0.9. Pt dispersions were measured via CO pulse chemisorption on a Quantachrome ChemBET 3000 system. Samples were reduced at 300 °C under flowing hydrogen (20 mL min^{-1}) for 1 h before room temperature analysis; this reduction protocol is identical to that employed for in situ pre-treatment prior to catalyst testing. A CO:Pt surface stoichiometry of 0.68 was assumed, since the formation of a fully saturated monolayer is energetically unfavorable as CO binds in an atop morphology, under the measurement conditions employed.[44] It is assumed CO binds only to the Pt under the conditions employed. Equations S1 and S2 in the supplementary information were used to estimate both the particle size (in the case of pure Pt) and surface Pt dispersion (for all samples containing sufficient platinum to measure).

Catalytic testing

In situ reduction and catalysis was carried out in a HEL multi-reactor high pressure platform (3 × 50 mL autoclaves). The catalyst of mass ~30 mg was heated under flowing H_2 to 300 °C at 5 °C min^{-1} and held for 0.5 h. This temperature was used as it is known that CuO will reduce in the temperature range 200–300 °C.[45-47] Upon cooling under flowing H_2, the autoclaves were purged and sealed with He to limit catalyst oxidation. While He was flowing, the reaction mixture consisting of methanol, (10 mL, Fisher Scientific, 99.99%) furfural (16.5 μL, 0.02 M, Sigma Aldrich) and internal standard, decane (38 μL, 0.02 M, Sigma Aldrich) was injected into each reactor. The mixture was allowed to degas for a period of 10 min before pressurizing under H_2 (1.5, 10 and 20 bar, BOC, 99.995%) and heating to 50 °C (stirring at 600 rpm). The reaction was continued for 7 h and sampled periodically by slowly depressurizing to atmospheric pressure and then re-pressurizing with H_2. Initial rate measurements were taken in quick succession from as low as 10 min after the start of the reactions until the first hour and subsequent samples were removed until the 7 h time point. Reaction samples were analysed offline on a Bruker Scion 456-GC equipped with a flame ionization detector and fitted with a Zebron ZB-5

(5%-phenyl-95%-dimethylpolysiloxane) capillary column. All peaks observed were validated by reference standards generated for the GC calibration.

Results and Discussion

Catalyst characterization

Table 1 shows a summary of the characterization results for all the catalysts used in this work, including metal loading as determined by ICP-OES, overall BET surface area, particle sizing by PXRD, TEM and CO chemisorption, surface metal ratios from XPS and finally Pt dispersion. Particle sizes obtained by TEM and PXRD for the Cu_{100} catalysts are in good agreement to each other. For the Pt_{100} although PXRD could not be used, particle size can additionally be estimated from CO chemisorption and this was in reasonable agreement with the TEM derived size. The equations used to calculate dispersion and particle size from CO titrations are shown in the supplementary information (Equation S1 and S2). Representative TEM images for the bimetallic and UDA catalysts with accompanying particle size histograms are shown in the supplementary information (Figure S2).

Table 1 - Comparative textural information for the monometallic and bimetallic and UDA Pt_xCu_{1-x}/γ-Al_2O_3 catalysts, presenting metal loading, overall BET surface area, particle size (PXRD, TEM and CO chemisorption), surface metallic ratios and Pt dispersion on the surface of the catalyst.

Catalyst	Pt wt%[a]	Cu wt%[a]	Surface area ($m^2\ g^{-1}$)	PXRD particle Size[b] (nm)	TEM particle Size (nm)	CO titration particle size (nm)[d]	Surface metallic ratios[c] (at%)		Pt dispersion by CO titration (%)[d]
							Pt	Cu	
Cu_{100} (Monometallic)	-	0.71	33	5.8	6.4 ± 1.6	-	-	100	-
Pt_1Cu_{20} (Ultra-Dilute Alloy)	0.09	0.59	33	6.0	5.2 ± 1.8	-	14	86	-
$Pt_{18}Cu_{82}$ (Alloy)	0.24	0.36	28	7.9	6.3 ± 1.8	-	21	79	29.4
$Pt_{38}Cu_{62}$ (Alloy)	0.53	0.28	31	8.4	6.9 ± 3.4	-	37	63	20.1
Pt_{100} (Monometallic)	1.20	-	39	-	4.4 ± 0.8	3.0	100	-	13.4

a – metal loading as determined by ICP-OES; b – Particle size as estimated by the Scherrer equation after the catalyst was reduced at 300 °C for 3 h; c – Surface atomic loading after reducing at 300 °C, as determined by XPS; d – Pt dispersion and CO titration particle size determined by CO chemisorption.

ICP-OES of the bimetallic catalysts found that there were decreases in Pt content, as expected, compared to the Pt_{100} catalyst. BET surface area measurements show that all the catalysts are broadly similar (Table 1). Surface metal compositions as determined by XPS were in agreement with bulk molar ratios determined by ICP-OES of Pt and Cu for the $Pt_{18}Cu_{82}$ and $Pt_{38}Cu_{62}$ samples, confirming the surface layers of the as reduced catalysts have the same composition as the bulk average. In contrast, the Pt_1Cu_{20} sample shows enrichment at the surface with a Pt:Cu ratio of relative 1:6 compared to 1:20 in the bulk. This is consistent with the preparation method using galvanostatic replacement of surface atoms. CO-titration derived Pt dispersion shows that as the Pt content is decreased, the overall dispersion and effectively the amount of surface Pt appears to increase slightly from 13.4% (Pt_{100}), to 20.1% ($Pt_{38}Cu_{62}$) and 29.4% ($Pt_{18}Cu_{82}$). However, it must be born in mind the surface stoichiometry of CO:Pt may increase beyond 2/3 (assumed in the dispersion calculation) for Pt atoms sited in a copper surface, so given the XPS shows no substantive change in surface composition from the bulk, this finding should be treated with caution. Nevertheless, the absence of a dramatic change in the Pt dispersion measurements for the alloys does show there is no substantial core-shell type effect and the Pt distribution appears roughly homogeneous – a conclusion further supported by the PXRD data presented later on. Both PXRD derived sizes and TEM data broadly agree and show the $Pt_{38}Cu_{62}$ and $Pt_{18}Cu_{82}$ alloys were similar in size to each other and the pure Cu particles.

Figure 1 shows PXRD diffractograms of the materials after calcination (Figure 1a) and after reduction (Figure 1b). Unassigned reflections correspond to trace amounts of δ-Al_2O_3 impurities in the Al_2O_3 support. It should be noted that both the Pt (111) and (200) reflections, expected at 39.8° and 47.4° 2-theta respectively, are unfortunately obscured by the Al_2O_3 support. However, for pure copper the (111) reflection is expected at 43.3°, and thus readily visible. After calcination, the only reflections seen are those due to the Al_2O_3 support. This is likely due to the copper component being oxidized and either amorphous or again obscured by the Al_2O_3 support. There has been no discernible modification to the γ-Al_2O_3 (for example, spinel formation) upon heating of the samples. Note, there is no Pt_1Cu_{20} calcined sample due to Pt being introduced after the Cu/Al_2O_3 was reduced. After reduction, a clear additional reflection

is seen in each of the patterns from all the Cu containing samples, shifting to lower 2-theta values with increasing Pt content. Figure 1c shows the variation in the position of this reflection as a function of Pt fraction, as compared to the positions expected in a uniform bulk alloy based on Vegard's law. The Cu_{100}, Pt_1Cu_{20} (which is almost pure copper) and $Pt_{18}Cu_{82}$ lie on precisely the expected line for bulk alloys, with the $Pt_{38}Cu_{62}$ sample suggesting the diffracting component has a slightly lower than expected Pt content (likely indicative of some slight Pt segregation – either in separate particles of via intraparticle separation such as core-shell formation). However, overall the PXRD data clearly point to the formation of well-mixed alloys in these samples.

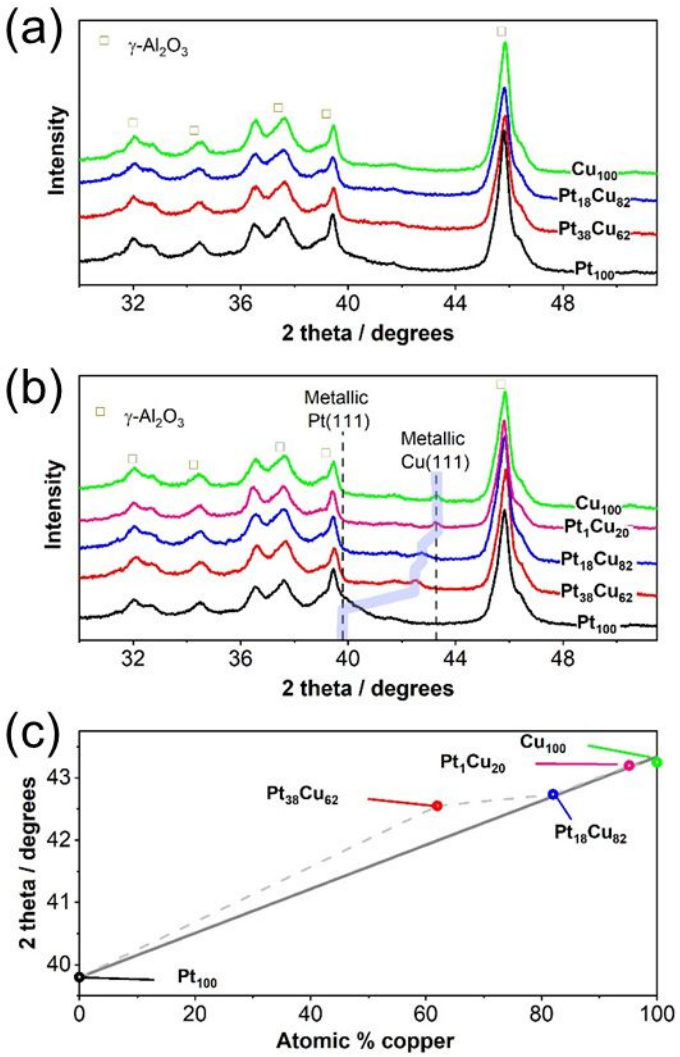

Figure 1 – PXRD diffractograms of supported monometallic, bimetallic and UDA catalysts after (a) calcination at 300 °C in air; (b) after reduction at 300 ° C in H_2 marking the Pt(111) and Cu(111) literature positions, and highlighting (lilac) the position of observed metallic reflections; (c) plot of actual vs expected 2-theta positions of the metallic (111) reflection based on Vegard's law (grey solid line shows expected positions). Note the

UDA, Pt_1Cu_{20}, is synthesised after the reduction step, so the after calcination sample in (a) is the same as for Cu_{100}.

Representative TEM images of the reduced monometallic $Pt_{100}/\gamma\text{-}Al_2O_3$ and $Cu_{100}/\gamma\text{-}Al_2O_3$ are shown in Figures 2a and 2b respectively. It is worth noting that due to the different Z-contrast between the heavier Pt and the lighter Cu, the nanoparticles in the two cases appear differently under the electron beam. Pt with an atomic number of 78 appears with far greater contrast compared to Cu, which has an atomic number of 29.[48] Consequently, these small copper particles can only be seen successfully at higher resolution as individual particles in bright field mode. Size distribution histograms, presented as insets in Figures 2a and 2b, show an average particle size and distribution of 4.4 ± 0.8 nm for the monometallic Pt catalyst and 6.4 ± 1.6 nm for the monometallic Cu catalyst. The narrow distribution observed in the case of Pt indicates that the nanoparticles are relatively homogenous in size and that they are thermally stable during calcination and reduction. In the case of Cu (Figure 2b) the nanoparticles are marginally larger and have a slightly broader distribution.

TEM supported by Energy Dispersive Spectroscopy (EDS) was carried out on the bimetallic alloy particles. Figure S1 shows a typical image of a singular $Pt_{38}Cu_{62}$ particle where there is a random dispersion of Cu (yellow) and Pt (blue), no areas of high concentration of a specific metal are evident. The atomic ratio of Cu and Pt for this particle was found to be 48:52. Other regions scanned showed similar atomic ratios, which were also accompanied by some particles with a slightly greater Cu content than Pt (consistent with the bulk ratio determined by ICP-OES). The maximum Cu content for a single bimetallic particle seen was ~70%. There were no particles observed to be rich in Pt, indicating the segregation noted above is probably due to intraparticle segregation, although more detailed investigation is outside the scope of the present work. The key point is that the microscopy is consistent with other techniques in demonstrating unambigously the reduced samples used for catalysis contain intimately mixed alloys with a local composition similar to that obtained by bulk elemental analysis of the sample.

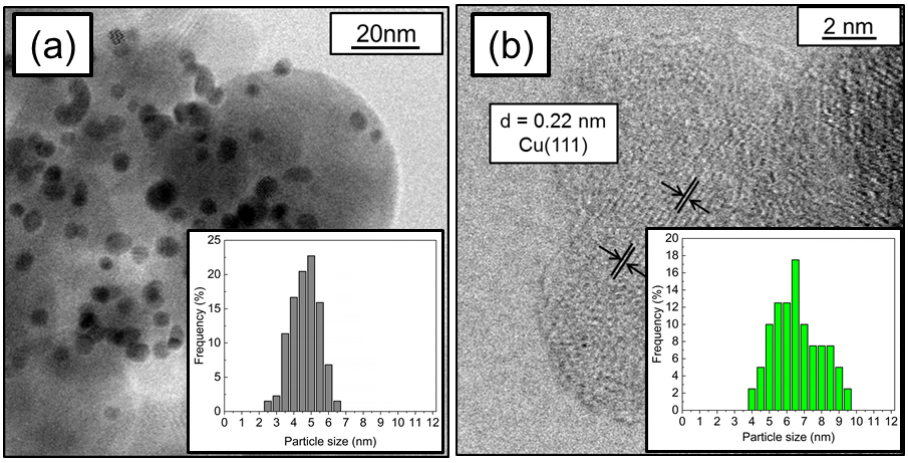

Figure 2 – (a) Shows a typical TEM image of Pt/γ-Al_2O_3 with corresponding histogram, (b) presents a HRTEM image of Cu/γ-Al_2O_3 with a histogram as well as interplanar measurements of the Cu(111) facet.

For the Pt_1Cu_{20} UDA sample, STEM HAADF images in Figure 3 (Bright (a,c) and Dark field (b,d)) were obtained. Due to the much higher atomic number of Pt, it is expected to show as a much brighter contribution than Cu in the (HAADF) dark-field images (b and d) (expected Rutherford scattering ratio ~7:1). The first observation is there is a not a distinctly brighter region of the particle, implying the Pt is not significantly segregated into a cluster, but likely well-dispersed. It is an instructive thought experiment to consider the numbers of Pt vs Cu atoms being viewed. For instance, for the particle shown in Figure 3d (on the small tail of the size distribution (for ease of imaging, about 3 nm). Assuming a spherical particle this can be expected to have of order 1200 atoms in total, with less than 60 Pt atoms. Assuming a surface thickness similar to a close-packed crystalline layer, around 460 of the atoms are at the surface. Even if all the Pt is at the surface, 88% of the surface atoms are Cu. The particle being viewed is probably around 10-20 atoms deep at the center (depending on assumptions made about shape and orientation). The key point is the concentration of Pt in this sample is so low, even if Pt may be at the surface it isn't a thin layer, and when viewed in transmission so few Pt atoms are present that a "bright-halo" around the edge of the particle is not expected, as seen for example in the surface segregation of Pt in PtCo nanoparticles.[49] The primary point is that in the case of Pt_1Cu_{20} catalyst significant Pt clustering or segregation could not be observed although the presence of small clusters cannot be excluded.

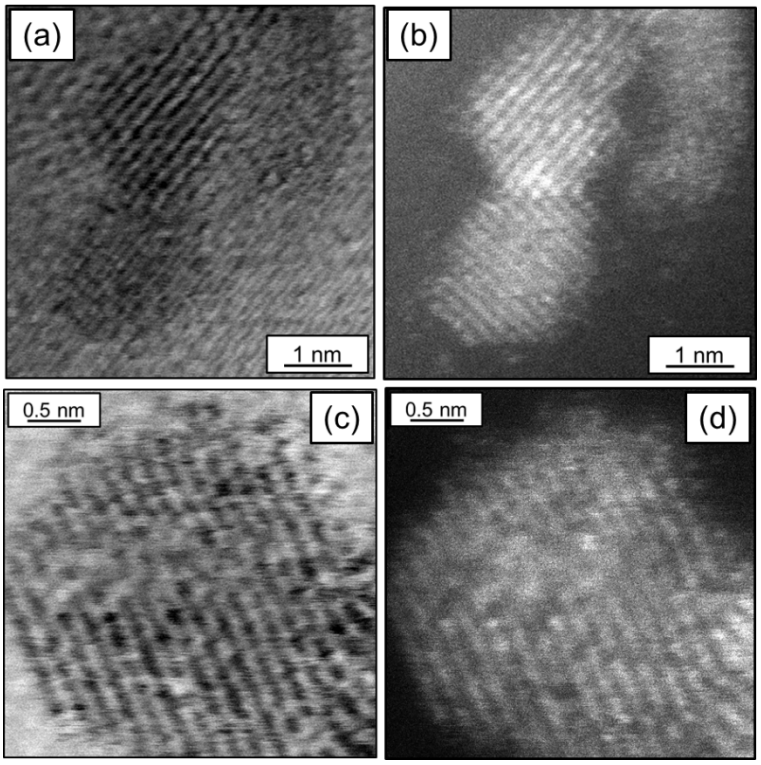

Figure 3 – Bright (a, c) and dark field (b, d) HAADF images of nanoparticles supported on γ-Al_2O_3 for the Pt_1Cu_{20} catalyst. Due to the change of Z contrast between the species.

XP spectra of the reduced samples are shown in Figure 4. The Cu_{100} and Pt_{100} catalysts align well with reported reference data for Cu and Pt metallic foils. The addition of Pt to Cu in all cases ($Pt_{38}Cu_{62}$, $Pt_{18}Cu_{82}$ and Pt_1Cu_{20}) results in a shift of the Cu 2p to slightly lower binding energy and the Pt 4d to slightly higher binding energy, indicative of electron transfer from Pt to Cu. While this is the reverse of what would be expected in the bulk from their Pauling electronegativities of 2.28 and 1.90 for Pt and Cu, respectively, XPS is dominated by the surface and electronegativities are known to differ within a few layers of the surface as a result of both different orbital involvement at an interface and differing surface atom densities due to lattice mismatching between two metals, as seen for overlayers of one metal on another.[50] This has specifically been seen for the case of a Cu adlayer on Pt(111), where the Cu core-level binding energy decreased by 0.27 eV.[51] The negative shifts seen in the Cu 2p level indicate a Pt-induced increase in the Cu electron population. For example, the atomic Cu $3d^94s^2$ to Cu $3d^{10}4s^1$ rehybridization is expected to give negative shifts in the binding energy for both core and d-valence levels while the Pt $5d^96s^1$ to Pt $5d^86s^2$ rehybridization will result in positive shifts. Thus, the primary charge transfer mechanism involves the Cu s,p electron donation, Pt d back

donation.[52-54] Similar shifts are seen for other PtCu bimetallic samples.[55-58] It should be noted the signal for Pt 4d is weaker than Pt 4f that would typically be used for such characterization, but the latter could not be separated from the alumina support contribution in that region]. The XP spectra also point to the absence of CuO in all the samples studied, which would be expected to be accompanied by satellites in the Cu 2p spectra between the Cu 2p spin-orbit pair and a higher Cu 2p binding energy. In all cases attempts to fit the spectra did not justify more than one component being present, as might reasonably be expected for reduced samples.

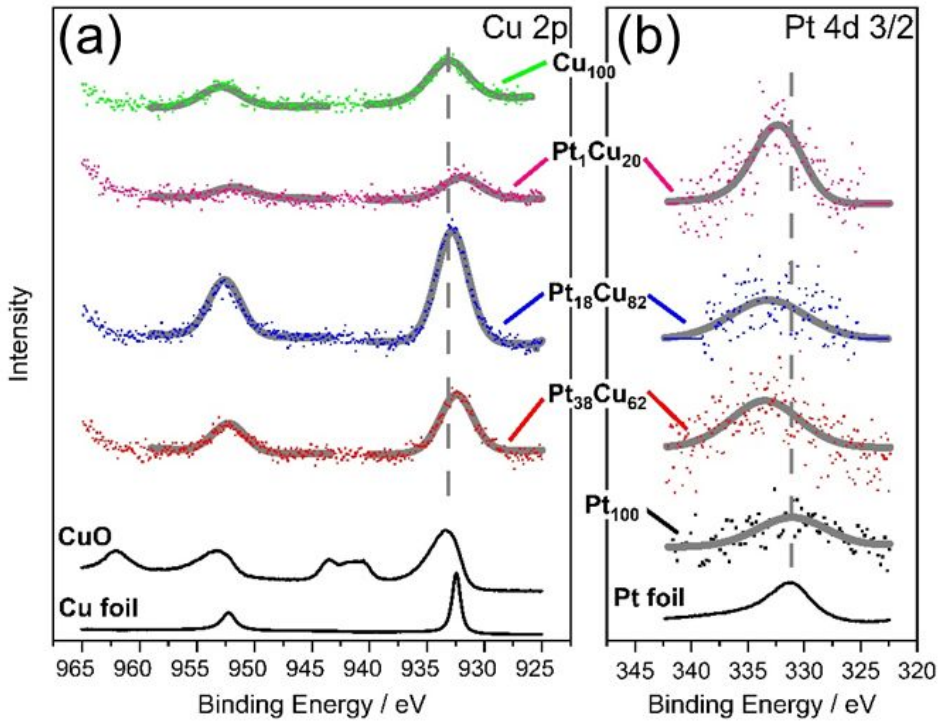

Figure 4 – XP spectra of catalyst samples after reduction where (a) is the Cu 2p doublet and (b) is the Pt $4d_{3/2}$ region. The dashed vertical lines are a guide to the eye at the peak centres for Cu_{100} and Pt_{100}. Reference spectra are shown in black lines for metallic Cu and Pt foil and CuO.

Catalyst reactivity

The supported monometallic reference catalysts Cu_{100} and Pt_{100}, along with the three bimetallic compositions, $Pt_{38}Cu_{62}$, $Pt_{18}Cu_{82}$ and Pt_1Cu_{20} were tested under batch conditions at three hydrogen pressures (1.5, 10 and 20 bar), using temperature and solvent reaction environments optimized previously.[16] Figure 5 shows the reaction profiles as a function of time for the three pressures, as well as the platinum mass normalized initial rates for all samples. By normalizing for Pt mass,

the effect of Pt dilution on the catalytic activity of PtCu alloys can be observed, especially for the case of Pt_1Cu_{20} where the effect of atomic Pt on a host Cu nanoparticle is scrutinised. Clearly, Pt (black) outperforms Cu (green) by about 1 order of magnitude at all pressures, as expected. This is highlighted in more detail in Figure S3. The overall furfural conversions taken at 7 h and reaction selectivities are presented in Figure 6. Additionally, post reaction catalysts were reclaimed and digested to assess stability to leaching/loss of metal via ICP-OES, this found that there were no substantial losses, as shown in Table S1.

For Pt_{100}, the reaction is near fully selective to furfural hydrogenation, with limited (<1%) presence of furan in the products. Furan is thought to be formed via a decarbonylation pathway and may be indicative of Pt deactivation via CO blocking active sites, especially for Pt(111).[16, 59, 60] Additionally, due to the use of previously optimized solvent and temperature conditions, no solvent coupled products were detected, a common issue with liquid phase furfural transformations.[16, 27] However, as the pressure used increases to 20 bar and almost complete conversion is reached, there is a very low concentration (~0.2 % selectivity) of tetrahydrofurfuryl alcohol (THFA) produced due to C=C hydrogenation (Scheme 1). This is a very modest amount of THFA compared to reactions in the literature using Pd.[30] In contrast the Cu_{100} catalyst formed furan as the major product when operating at 1.5 bar and in discernible quantities at higher pressures. There are selectivity differences to our previous work due to the different preparation methods for Cu/Al_2O_3 catalysts, although interestingly a very similar overall activity is observed at 1.5 bar H_2.[8]

For the alloy samples $Pt_{38}Cu_{62}$ and $Pt_{18}Cu_{82}$, the high conversion of Pt_{100} is mostly preserved, dropping only slightly at the lowest pressure, although on dilution to 18% Pt, the selectivity at lower pressures starts to decrease with the production of furan (similar to pure copper). It is likely that hydrogenation over these samples proceeds via a spillover pathway, whereby the hydrogen dissociates at Pt sites and spills over onto nearby copper sites, where furfural can be absorbed and hydrogenated without the need for Pt.[42, 61] A drop in furfural conversion is shown for the alloy catalysts at 20 bar which is attributed to a surface saturation of H_2. As previously shown in our work on a model Pt(111) surface, furfural adsorption can be restricted

by H_2 crowding decreasing catalyst turnover.[23] Note, the alloys $Pt_{38}Cu_{62}$ and $Pt_{18}Cu_{82}$ produced a slightly larger THFA selectivity than Pt on its own, 0.9% and 0.8%, respectively when operating at 20 bar. This increase in selectivity is a far milder effect than previously shown for PtNi alloys which has been found to drive to reaction towards THFA formation.[38]

For the UDA catalyst Pt_1Cu_{20}, at 10 and 20 bar the high conversion is maintained, but it exhibits only very low activity at 1.5 bar. From the reaction profiles in Figure 5b and c, the Pt_1Cu_{20} sample exhibits a clear induction period (~0.7 h at 20 bar, 2 h at 10 bar) under conditions where it is active. After this induction period, it exhibits a rate per platinum atom higher than any other catalyst including Pt_{100} (Figure 5d), and remains strikingly selective to the desired furfuryl alcohol product. Speculatively, the induction could result from a number of possibilities. The first is the reduction of a small quantity of surface copper oxide, however, given the in situ reduction employed before reaction and the lack of evidence for copper oxides this can be reasonably discounted. A second alternative is hydrogen-induced migration of Pt to the surface. This process, where individual Pt atoms that possess a higher surface energy than the Cu host migrate up through the bulk to the surface in the presence of H_2 has been reported previously.[62] Theoretical work supports Pt being more stable in the bulk than on the surface in the absence of any external stimuli (e.g. hydrogen pressure), showing that the surface energy per atom in a (111) array is ~0.70 eV for Cu vs ~1.0 eV for Pt (which remains higher even accounting for the slightly larger size of the Pt).[63, 64] However, the presence of a significant Pt enrichment at the surface by XPS in the 'as reduced' sample (also consistent with the fact the sample was prepared by 'surface displacement') suggests surface migration alone is also unlikely to account for the induction. A third possibility is the formation of appropriate ensembles on the surface may be necessary – the cluster size needed for hydrogen activation has been investigated by Gates and co-workers [65] as well as Cao et al [66] for bimetallics, including PtCu, and those in a small size (~1.5 nm) by Chandler and co-workers.[67] They proposed the need for a minimum surface Pt ensemble to activate hydrogen in the PtCu catalyzed toluene reduction. In the present work the substantial dilution of Pt affords the same low probability of surface platinum ensembles occurring at random – but such clustering could be induced by hydrogen.

Further work is needed to investigate such effects, but the presence of this induction process is an interesting aside.

A second important observation is the absolute rates of conversion (not just the Pt normalized rate), appear higher with Pt_1Cu_{20} than for the pure Pt catalyst (note the steep rise after induction, Figures 5b and 5c). It is possible that the presence of Pt even at this dilution—which for a 6 nm particle corresponds to at most ~20% of the surface atoms—still alters the adsorption strength or geometry. The adsorption energies of furfural on Cu(111) and Pt(111) are predicted to be quite different, 0.47 eV and 1.07 eV, respectively,[68] and differences in furfural's adsorption geometry are known to effect reactivity.[23, 35, 69] For Cu this involves the interaction of the lone pair on the furfural molecule with the Cu(111) surface, resulting in a perpendicular η^1(O)-aldehyde conformation, opposed to the parallel η^2(C, O)-aldehyde conformation for Pt. This conformation is preferred due to the repulsion of the aromatic furan ring from the closely-packed Cu(111) surface which was assumed by Sitthisa et al. to arise from the overlap of the antibonding orbitals of the furan ring and the 3d band of the Cu surface atoms.[70] While Cu surfaces can facilely adsorb furfural, reaction progression can be hampered by a large activation barrier for hydrogen dissociative adsorption.[33]In contrast, the presence of Pt in the UDA catalyst can facilitate hydrogen dissociative adsorption and spillover onto the Cu as it has been seen for similar systems.[33, 71-74] Through this work a route to bridge model catalytic systems and real world catalysts can be found for an ultra-dilute Pt species. The adsorbed hydrogen preferentially interacts with the oxygen atom of the carbonyl. [70] It is important to note that the filled d-valence band of Cu leads to an unfavorable interaction with the furanic ring of furfural caused by the repulsion between the occupied furfural π orbitals. Thus, the interaction of furfural on Cu via η^1(O) or η^2(C,O) configuration is enhanced, which results in activation of C=O bond favoring C=O hydrogenation. As a result, it is also likely (based on the low selectivity to furan) that there may be inhibition of CO poisoning afforded by the copper matrix, as has been reported for 'single atom alloy' catalysts.[59, 75, 76] Overall however, the critical point is the comparison (Figure 5d) of activity normalized to Pt amount, which clearly shows ultra-dilute catalysts have the potential to enable us to efficiently use the scarce resource of precious metals in a way that

isn't achieved by near stoichiometric alloys and outperforms (very significantly under some conditions) the platinum efficiency of the pure Pt catalyst.

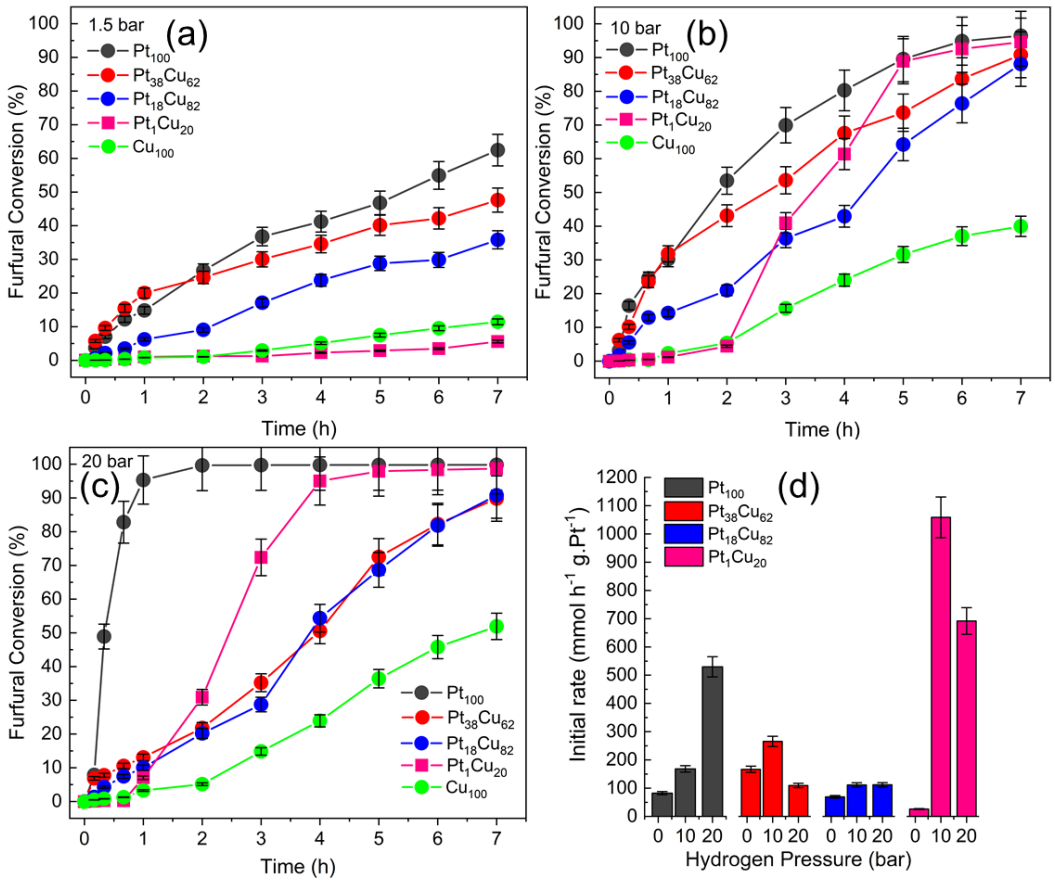

Figure 5 – Reactivity of all the catalysts used at (a) 1.5 bar, (b) 10 bar and (c) 20 bar. Additionally, (d) normalized initial rates per gram of Pt_{100} for Pt, $Pt_xCu_{(1-x)}$ and Pt_1Cu_{20} catalysts across the 3 hydrogen pressures.

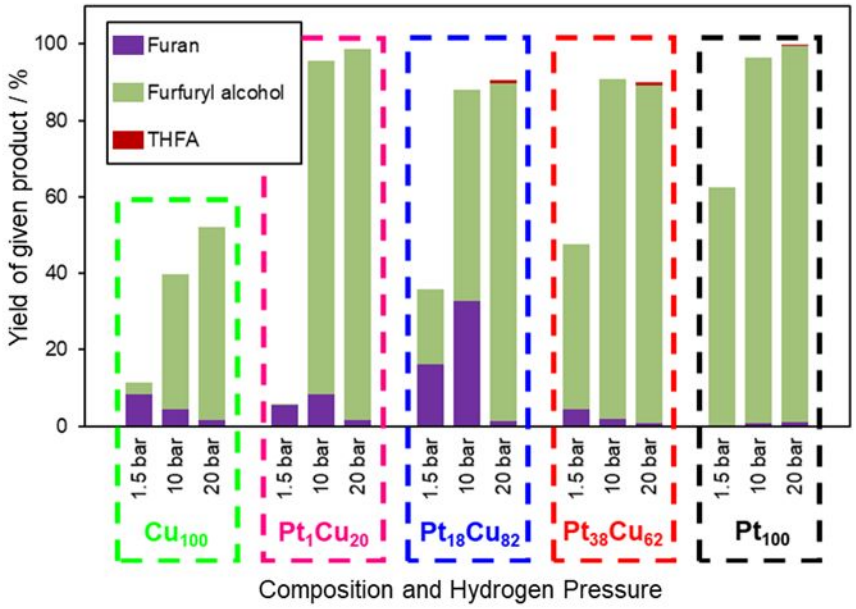

Figure 6 – Showing conversion and selectivity as an overall yield for each catalyst sample across three hydrogen pressures studied at 50 °C in methanol after 7 h. THFA = Tetrahydrofurfuryl alcohol.

Conclusions

PtCu bimetallic alloy catalysts, including an "Ultra-Dilute" Alloy (UDA, 1:20 atomic ratio) catalyst all exhibit higher reactivity for furfural hydrogenation than pure copper. The UDA catalyst at 10 and 20 bar is nearly as selective as pure Pt, but (after a brief induction period) exhibits much higher per platinum atom activities, making better use of scarce precious metal resources. The surface metal compositions determined by XPS compared well with ICP-OES analysis of the metal ratios present and the synthesis method used, and PXRD shows the catalysts broadly follow the expected trend for their alloy compositions. XPS additionally demonstrated an electronic interaction occurred in all three alloy samples, demonstrated by shifts in the Cu 2p and correspondingly in the Pt 4d indicating Pt→Cu electron transfer had occurred. As the best operating reaction conditions for this system are still relatively mild in comparison with those seen for the industrial copper chromite standard (typically >200 °C, ~30 bar), and these materials make more efficient use of scarce Pt than other precious metal catalysts reported, the data has shown that $Pt_xCu_{(1-x)}$ bimetallic catalysts, especially at high Pt dilution, are a promising, green and environmentally friendly alternative in the push to switch to bio-renewable chemical feedstocks.

ASSOCIATED CONTENT

Additional TEM/EDX, catalyst reactivity data, post reaction ICP data and calculations are provided in the supporting information.

Corresponding Author

Email: kyriakg@upatras.gr

Acknowledgements

MJT acknowledges funding through the THYME project (UKRI, Research England). GK acknowledges funding from EPSRC (EP/M005186/1). GK and ST acknowledge funding by the University of Patras Research Committee under the basic research program K. Karatheodoris.

References

[1] M.J. Taylor, H.A. Alabdrabalameer, V. Skoulou, Choosing Physical, Physicochemical and Chemical Methods of Pre-Treating Lignocellulosic Wastes to Repurpose into Solid Fuels, Sustainability, 11 (2019) 3604.
[2] R. Mariscal, P. Maireles-Torres, M. Ojeda, I. Sádaba, M. López Granados, Furfural: a renewable and versatile platform molecule for the synthesis of chemicals and fuels, Energy & Environmental Science, 9 (2016) 1144-1189.
[3] J.J. Bozell, G.R. Petersen, Technology development for the production of biobased products from biorefinery carbohydrates—the US Department of Energy's "Top 10" revisited, Green Chemistry, 12 (2010) 539.
[4] A. Mandalika, L. Qin, T.K. Sato, T. Runge, Integrated biorefinery model based on production of furans using open-ended high yield processes, Green Chem., 16 (2014) 2480-2489.
[5] M. Besson, P. Gallezot, C. Pinel, Conversion of biomass into chemicals over metal catalysts, Chem. Rev 114 (2014) 1827-1870.
[6] K.J. Zeitsch, The Chemistry and Technology of Furfural and Its Many By-Products, (2000) 375.
[7] K. Yan, G. Wu, T. Lafleur, C. Jarvis, Production, properties and catalytic hydrogenation of furfural to fuel additives and value-added chemicals, Renewable Sustainable Energy Rev., 38 (2014) 663-676.
[8] M.J. Islam, M. Granollers Mesa, A. Osatiashtiani, M.J. Taylor, J.C. Manayil, C.M.A. Parlett, M.A. Isaacs, G. Kyriakou, The effect of metal precursor on copper phase dispersion and nanoparticle formation for the catalytic transformations of furfural, Applied Catalysis B: Environmental, (2020).
[9] R.V. Sharma, U. Das, R. Sammynaiken, A.K. Dalai, Liquid phase chemo-selective catalytic hydrogenation of furfural to furfuryl alcohol, Appl. Catal. A Gen, 454 (2013) 127-136.
[10] D. Vargas-Hernández, J.M. Rubio-Caballero, J. Santamaría-González, R. Moreno-Tost, J.M. Mérida-Robles, M.A. Pérez-Cruz, A. Jiménez-López, R. Hernández-Huesca, P.

Maireles-Torres, Furfuryl alcohol from furfural hydrogenation over copper supported on SBA-15 silica catalysts, J. Mol. Catal. A: Chem., 383-384 (2014) 106-113.
[11] O.F. Aldosari, S. Iqbal, P.J. Miedziak, G.L. Brett, D.R. Jones, X. Liu, J.K. Edwards, D.J. Morgan, D.K. Knight, G.J. Hutchings, Pd-Ru/TiO2 catalyst - an active and selective catalyst for furfural hydrogenation, Catal. Sci. Technol., 6 (2016) 234-242.
[12] D. Liu, D. Zemlyanov, T. Wu, R.J. Lobo-Lapidus, J.A. Dumesic, J.T. Miller, C.L. Marshall, Deactivation mechanistic studies of copper chromite catalyst for selective hydrogenation of 2-furfuraldehyde, J. Catal., 299 (2013) 336-345.
[13] K. Egeblad, J. Rass-Hansen, C. Marsden, E. Taarning, C. Hviid, Heterogeneous catalysis for production of value-added chemicals from biomass, Catalysis: Volume 21, Royal Society Of Chemistry, 2008, pp. 13-50.
[14] A.S. Gowda, S. Parkin, F.T. Ladipo, No Title, Appl. Organomet. Chem 26 (2012) 86-93.
[15] S. Bhogeswararao, D. Srinivas, Catalytic conversion of furfural to industrial chemicals over supported Pt and Pd catalysts, J. Catal., 327 (2015) 65-77.
[16] M.J. Taylor, L.J. Durndell, M.A. Isaacs, C.M.A. Parlett, K. Wilson, A.F. Lee, G. Kyriakou, Highly selective hydrogenation of furfural over supported Pt nanoparticles under mild conditions, Appl. Catal. B Environ, 180 (2016) 580-585.
[17] M. Audemar, C. Ciotonea, K. De Oliveira Vigier, S. Royer, A. Ungureanu, B. Dragoi, E. Dumitriu, F. Jerome, Selective Hydrogenation of Furfural to Furfuryl Alcohol in the Presence of a Recyclable Cobalt/SBA-15 Catalyst, ChemSusChem, 8 (2015) 1885-1891.
[18] M.M. Villaverde, N.M. Bertero, T.F. Garetto, A.J. Marchi, Selective liquid-phase hydrogenation of furfural to furfuryl alcohol over Cu-based catalysts, Catal. Today, 213 (2013) 87-92.
[19] R.M. Mironenko, O.B. Belskaya, T.I. Gulyaeva, A.I. Nizovskii, A.V. Kalinkin, V.I. Bukhtiyarov, A.V. Lavrenov, V.A. Likholobov, Effect of the nature of carbon support on the formation of active sites in Pd/C and Ru/C catalysts for hydrogenation of furfural, Catal. Today, 249 (2015) 145-152.
[20] P. Reyes, D. Salinas, C. Campos, M. Oportus, Selective hydrogenation of furfural on Ir/TiO2 catalysts, Quim. Nova, 33 (2010) 777-780.
[21] V. Vetere, A.B. Merlo, J.F. Ruggera, M.L. Casella, Transition metal-based bimetallic catalysts for the chemoselective hydrogenation of furfuraldehyde, J. Braz. Chem. Soc, 21 (2010) 914-920.
[22] K.L. MacIntosh, S.K. Beaumont, Nickel-Catalysed Vapour-Phase Hydrogenation of Furfural, Insights into Reactivity and Deactivation, Topics in Catalysis, (2020).
[23] M.J. Taylor, L. Jiang, J. Reichert, A.C. Papageorgiou, S.K. Beaumont, K. Wilson, A.F. Lee, J.V. Barth, G. Kyriakou, Catalytic Hydrogenation and Hydrodeoxygenation of Furfural over Pt(111): A Model System for the Rational Design and Operation of Practical Biomass Conversion Catalysts, J Phys Chem C, 121 (2017) 8490-8497.
[24] K. An, N. Musselwhite, G. Kennedy, V.V. Pushkarev, L.R. Baker, G.A. Somorjai, Preparation of mesoporous oxides and their support effects on Pt nanoparticle catalysts in catalytic hydrogenation of furfural., J. Colloid Interface Sci., 392 (2013) 122-128.
[25] O. Deutschmann, Knözinger, H., Kochloefl, K. and Turek, T, Heterogeneous Catalysis and Solid Catalysts, (2009) 110.
[26] S. Srivastava, G.C. Jadeja, J. Parikh, A versatile bi-metallic copper-cobalt catalyst for liquid phase hydrogenation of furfural to 2-methylfuran, RSC Advances, 6 (2016) 1649-1658.

[27] A.B. Merlo, V. Vetere, J.M. Ramallo-López, F.G. Requejo, M.L. Casella, Liquid-phase furfural hydrogenation employing silica-supported PtSn and PtGe catalysts prepared using surface organometallic chemistry on metals techniques, React. Kinet. Mechanism Catal., 104 (2011) 467-482.
[28] A.B. Merlo, V. Vetere, J.F. Ruggera, M.L. Casella, Bimetallic PtSn catalyst for the selective hydrogenation of furfural to furfuryl alcohol in liquid-phase, Catal. Commun, 10 (2009) 1665-1669.
[29] Z.L. Wu, J. Wang, S. Wang, Y.-X. Zhang, G.-Y. Bai, L. Ricardez-Sandoval, G.-C. Wang, B. Zhao, Controllable chemoselective hydrogenation of furfural by PdAg/C bimetallic catalysts under ambient operating conditions: an interesting Ag switch, Green Chem., 22 (2020) 1432-1442.
[30] K. Fulajtárova, T. Soták, M. Hronec, I. Vávra, E. Dobročka, M. Omastová, Aqueous phase hydrogenation of furfural to furfuryl alcohol over Pd-Cu catalysts, Applied Catalysis A: General, 502 (2015) 78-85.
[31] B. Chen, F. Li, Z. Huang, G. Yuan, Tuning catalytic selectivity of liquid-phase hydrogenation of furfural via synergistic effects of supported bimetallic catalysts, Applied Catalysis A: General, 500 (2015) 23-29.
[32] S.T. Thompson, H.H. Lamb, Palladium–Rhenium Catalysts for Selective Hydrogenation of Furfural: Evidence for an Optimum Surface Composition, ACS Catal., 6 (2016) 7438-7447.
[33] G. Kyriakou, M.B. Boucher, A.D. Jewell, E.A. Lewis, T.J. Lawton, A.E. Baber, H.L. Tierney, M. Flytzani-Stephanopoulos, E.C.H. Sykes, Isolated metal atom geometries as a strategy for selective heterogeneous hydrogenations., Science (New York, N.Y.), 335 (2012) 1209-1212.
[34] M.V. Twigg, M.S. Spencer, Deactivation of supported copper metal catalysts for hydrogenation reactions, Applied Catalysis a-General, 212 (2001) 161-174.
[35] S.M. Rogers, C.R.A. Catlow, C.E. Chan-Thaw, A. Chutia, N. Jian, R.E. Palmer, M. Perdjon, A. Thetford, N. Dimitratos, A. Villa, P.P. Wells, Tandem Site and Size Controlled Pd Nanoparticles for the Directed Hydrogenation of Furfural, ACS Catal, (2017).
[36] S. Chen, R. Wojcieszak, F. Dumeignil, E. Marceau, S. Royer, How Catalysts and Experimental Conditions Determine the Selective Hydroconversion of Furfural and 5-Hydroxymethylfurfural, Chem Rev, 118 (2018) 11023-11117.
[37] M. Lesiak, M. Binczarski, S. Karski, W. Maniukiewicz, J. Rogowski, E. Szubiakiewicz, J. Berlowska, P. Dziugan, I. Witońska, Hydrogenation of furfural over Pd–Cu/Al2O3 catalysts. The role of interaction between palladium and copper on determining catalytic properties, Journal of Molecular Catalysis A: Chemical, 395 (2014) 337-348.
[38] J. Wu, X. Zhang, Q. Chen, L. Chen, Q. Liu, C. Wang, L. Ma, One-Pot Hydrogenation of Furfural into Tetrahydrofurfuryl Alcohol under Ambient Conditions over PtNi Alloy Catalyst, Energy & Fuels, 34 (2019) 2178-2184.
[39] V.V. Pushkarev, N. Musselwhite, K. An, S. Alayoglu, G.A. Somorjai, High structure sensitivity of vapor-phase furfural decarbonylation/hydrogenation reaction network as a function of size and shape of Pt nanoparticles, Nano Lett, 12 (2012) 5196-5201.
[40] J.J. Corral-Pérez, C. Copéret, A. Urakawa, Lewis acidic supports promote the selective hydrogenation of carbon dioxide to methyl formate in the presence of methanol over Ag catalysts, Journal of Catalysis, 380 (2019) 153-160.

[41] M.T. Darby, F.R. Lucci, M.D. Marcinkowski, A.J. Therrien, A. Michaelides, M. Stamatakis, E.C.H. Sykes, Carbon Monoxide Mediated Hydrogen Release from PtCu Single-Atom Alloys: The Punctured Molecular Cork Effect, J. Phys. Chem. C, 123 (2019) 10419-10428.
[42] F.R. Lucci, M.D. Marcinkowski, T.J. Lawton, E.C.H. Sykes, H2 Activation and Spillover on Catalytically Relevant Pt–Cu Single Atom Alloys, The Journal of Physical Chemistry C, 119 (2015) 24351-24357.
[43] F.R. Lucci, J. Liu, M.D. Marcinkowski, M. Yang, L.F. Allard, M. Flytzani-Stephanopoulos, E.C.H. Sykes, Selective hydrogenation of 1,3-butadiene on platinum–copper alloys at the single-atom limit, Nat. Commun., 6 (2015) 8550.
[44] M. Panahi, N. Solati, S. Gürlek, H. Ogasawara, S. Kaya, Weakening the strength of CO binding on subsurface alloyed Pt(111), Surf. Sci., 682 (2019) 1-7.
[45] J. Pike, S.-W. Chan, F. Zhang, X. Wang, J. Hanson, Formation of stable Cu2O from reduction of CuO nanoparticles, Applied Catalysis A: General, 303 (2006) 273-277.
[46] Y. Li, Q. Fu, M. Flytzani-Stephanopoulos, Low-temperature water-gas shift reaction over Cu- and Ni-loaded cerium oxide catalysts, Applied Catalysis B-Environmental, 27 (2000) 179-191.
[47] L. Kundakovic, M. Flytzani-Stephanopoulos, Reduction characteristics of copper oxide in cerium and zirconium oxide systems, Applied Catalysis a-General, 171 (1998) 13-29.
[48] M.C. Akatay, W. Sinkler, S.I. Sanchez, S.A. Bradley, Z-contrast imaging for elemental analysis: Single atoms to clusters, Microsc. Microanal., 23 (2017) 482-483.
[49] S. Alayoglu, S.K. Beaumont, F. Zheng, V.V. Pushkarev, H. Zheng, V. Iablokov, Z. Liu, J. Guo, N. Kruse, G.A. Somorjai, CO_2 Hydrogenation Studies on Co and CoPt Bimetallic Nanoparticles Under Reaction Conditions Using TEM, XPS and NEXAFS, Top. Catal., 54 (2011) 778-785.
[50] J.A. Rodriguez, D.W. Goodman, The nature of the metal-metal bond in bimetallic surfaces, Science, 257 (1992) 897-903.
[51] J.A. Rodriguez, R.A. Campbell, D.W. Goodman, Electronic interactions in bimetallic systems: Core‐level binding energy shifts, Journal of Vacuum Science & Technology A, 9 (1991) 1698-1702.
[52] Y.S. Lee, K.Y. Lim, Y.D. Chung, C.N. Whang, Y. Jeon, XPS core‐level shifts and XANES studies of Cu–Pt and Co–Pt alloys, Surf. Interface Anal, 30 (2000) 475-478.
[53] J. A. Rodriguez, M. Kuhn, Electronic and Chemical Properties of Ag/Pt(111) and Cu/Pt(111) Surfaces: Importance of Changes in the d Electron Populations, J. Phys. Chem, 98, (1994) 11251-11255.
[54] N. T. Barrett, R. Belkhou, J. Thiele, C. Guillot, A core-level photoemission spectroscopy study of the formation of surface alloy Cu/Pt(111): comparison with Pt/Cu(111), Surf. Sci. 331-333 (1995) 776-781.
[55] W. Kang, R. Li, D. Wei, S. Xu, S. Wei, H. Li, CTAB-reduced synthesis of urchin-like Pt–Cu alloy nanostructures and catalysis study towards the methanol oxidation reaction, RSC Adv., 5 (2015) 94210-94215.
[56] A.L. Wang, C. Zhang, W. Zhou, Y.-X. Tong, G.-R. Li, PtCu alloy nanotube arrays supported on carbon fiber cloth as flexible anodes for direct methanol fuel cell, AIChE J., 62 (2016) 975-983.
[57] Z. Xu, H. Zhang, S. Liu, B. Zhang, H. Zhong, D.S. Su, Facile synthesis of supported Pt–Cu nanoparticles with surface enriched Pt as highly active cathode catalyst for proton exchange membrane fuel cells, Int. J. Hydrogen Energy, 37 (2012) 17978-17983.

[58] S.V. Myers, A.I. Frenkel, R.M. Crooks, X-ray Absorption Study of PdCu Bimetallic Alloy Nanoparticles Containing an Average of ~64 Atoms, Chem. Mater., 21 (2009) 4824-4829.
[59] J. Liu, F.R. Lucci, M. Yang, S. Lee, M.D. Marcinkowski, A.J. Therrien, C.T. Williams, E.C. Sykes, M. Flytzani-Stephanopoulos, Tackling CO Poisoning with Single-Atom Alloy Catalysts, J. Am. Chem. Soc., 138 (2016) 6396-6399.
[60] D.J. Davis, G. Kyriakou, R.M. Lambert, Uptake of n-hexane, 1-butene, and toluene by Au/Pt bimetallic surfaces: a tool for selective sensing of hydrocarbons under high-vacuum conditions, J Phys Chem B, 110 (2006) 11958-11961.
[61] S.K. Beaumont, S. Alayoglu, C. Specht, N. Kruse, G.A. Somorjai, A nanoscale demonstration of hydrogen atom spillover and surface diffusion across silica using the kinetics of CO2 methanation catalyzed on spatially separate Pt and Co nanoparticles, Nano Lett, 14 (2014) 4792-4796.
[62] Q. Fu, Y. Luo, Catalytic Activity of Single Transition-Metal Atom Doped in Cu(111) Surface for Heterogeneous Hydrogenation, J. Phys. Chem. C, 117 (2013) 14618-14624.
[63] H.L. Skriver, N.M. Rosengaard, Surface energy and work function of elemental metals, Physical Review B, 46 (1992) 7157-7168.
[64] L. Vitos, A.V. Ruban, H.L. Skriver, J. Kollar, The surface energy of metals, Surf. Sci., 411 (1998) 186-202.
[65] Z. Xu, F.S. Xiao, S.K. Purnell, O. Alexeev, S. Kawi, S.E. Deutsch, B.C. Gates, Size-dependent catalytic activity of supported metal clusters, Nature, 372 (1994) 346-348.
[66] Y. Cao, J. Guerrero-Sańchez, I. Lee, X. Zhou, N. Takeuchi, F. Zaera, Kinetic Study of the Hydrogenation of Unsaturated Aldehydes Promoted by CuPtx/SBA-15 Single-Atom Alloy (SAA) Catalysts, ACS Catalysis, 10 (2020) 3431-3443.
[67] B.D. Chandler, A.B. Schabel, L.H. Pignolet, Ensemble Size Effects on Toluene Hydrogenation and Hydrogen Chemisorption by Supported Bimetallic Particle Catalysts, J. Phys. Chem. B, 105 (2001) 149-155.
[68] B. Liu, L. Cheng, L. Curtiss, J. Greeley, Effects of van der Waals density functional corrections on trends in furfural adsorption and hydrogenation on close-packed transition metal surfaces, Surf. Sci, 622 (2014) 51-59.
[69] D. Shi, J.M. Vohs, Deoxygenation of Biomass-Derived Oxygenates: Reaction of Furfural on Zn-Modified Pt(111), ACS Catal., 5 (2015) 2177-2183.
[70] S. Sitthisa, T. Sooknoi, Y.G. Ma, P.B. Balbuena, D.E. Resasco, Kinetics and mechanism of hydrogenation of furfural on Cu/SiO2 catalysts, Journal of Catalysis, 277 (2011) 1-13.
[71] M. Luneau, J.S. Lim, D.A. Patel, E.C.H. Sykes, C.M. Friend, P. Sautet, Guidelines to Achieving High Selectivity for the Hydrogenation of alpha,beta-Unsaturated Aldehydes with Bimetallic and Dilute Alloy Catalysts: A Review, Chem Rev, (2020).
[72] R. Reocreux, P.L. Kress, R.T. Hannagan, V. Cinar, M. Stamatakis, E.C.H. Sykes, Controlling Hydrocarbon (De)Hydrogenation Pathways with Bifunctional PtCu Single-Atom Alloys, J Phys Chem Lett, 11 (2020) 8751-8757.
[73] R.T. Hannagan, G. Giannakakis, M. Flytzani-Stephanopoulos, E.C.H. Sykes, Single-Atom Alloy Catalysis, Chem Rev, (2020).
[74] M.D. Marcinkowski, M.T. Darby, J. Liu, J.M. Wimble, F.R. Lucci, S. Lee, A. Michaelides, M. Flytzani-Stephanopoulos, M. Stamatakis, E.C.H. Sykes, Pt/Cu single-atom alloys as coke-resistant catalysts for efficient C-H activation, Nat Chem, 10 (2018) 325-332.

[75] G. Giannakakis, M. Flytzani-Stephanopoulos, E.C.H. Sykes, Single-Atom Alloys as a Reductionist Approach to the Rational Design of Heterogeneous Catalysts, Acc. Chem. Res., (2018).
[76] K. Yuge, Y. Koyama, A. Kuwabara, I. Tanaka, Surface design of alloy protection against CO-poisoning from first principles, J Phys Condens Matter, 26 (2014) 355006.

TOC GRAPHIC